**Weierstraß-Institut**
**für Angewandte Analysis und Stochastik**

**Leibniz-Institut im Forschungsverbund Berlin e. V.**

Preprint ISSN 2198-5855

# Temporal solitons in an optically injected Kerr cavity with two spectral filters

Alexander Pimenov, Andrei G. Vladimirov

submitted: July 26, 2022

Weierstrass Institute
Mohrenstr. 39
10117 Berlin
Germany
E-Mail: alexander.pimenov@wias-berlin.de
andrei.vladimirov@wias-berlin.de

No. 2948
Berlin 2022

2010 *Physics and Astronomy Classification Scheme.* 42.65.Tg, 42.65.Pc, 42.65.Sf, 02.30.Ks.

*Key words and phrases.* Temporal cavity solitons, passive optical cavity, dispersion.

Authors acknowledge the support of the joint DFG-RSF Project 445430311.

Edited by
Weierstraß-Institut für Angewandte Analysis und Stochastik (WIAS)
Leibniz-Institut im Forschungsverbund Berlin e. V.
Mohrenstraße 39
10117 Berlin
Germany

Fax: +49 30 20372-303
E-Mail: preprint@wias-berlin.de
World Wide Web: http://www.wias-berlin.de/

# Temporal solitons in an optically injected Kerr cavity with two spectral filters

Alexander Pimenov, Andrei G. Vladimirov

**Abstract**

We investigate theoretically the dynamical behavior of an optically injected Kerr cavity where the chromatic dispersion is induced by propagation of light through two Lorentzian spectral filters with different widths and central frequencies. We show that this setup can be modeled by a second order delay differential equation that can be considered as a generalization of the Ikeda map with included spectral filtering, dispersion, and coherent injection terms. We demonstrate that this equation can exhibit modulational instability and bright localized structures formation in the anomalous dispersion regime.

## 1 Introduction

Time-delay models of optical systems like Ikeda map [1], Lang-Kobayashi equations [2], delay differential equation (DDE) mode-locked laser models [3, 4, 5, 6, 7, 8, 9, 10, 11], frequency swept laser models [12, 13], and others were successfully used to describe unidirectional propagation of light through linear and nonlinear optical elements in a ring cavity. Unlike Nonlinear Schrödinger (NLS)- or complex Ginzburg-Landau (CGL)-type equations these models are free from the mean field approximation and therefore are valid for arbitrary large gain and losses in the cavity. An important drawback of the time-delay models, however, is that the inclusion of an arbitrary second order chromatic dispersion of the intracavity media into these models is not a trivial task. Recently, it was shown that chromatic dispersion in photonic crystal mode-locked laser [14] and a SOA-fiber laser with fiber delay line [15] can be described using a distributed delay term, which arises from the transfer function of a detuned Lorentzian absorption line in frequency domain. Furthermore, under assumption of weak dispersion one can replace the distributed time delay model with an extended DDE model containing a single additional ordinary differential equation for the polarization variable [16]. Using this extended DDE model, the conventional combined effects of chromatic dispersion and nonlinearity such as modulational instability (MI) in the anomalous dispersion regime and bright localized structures formation were demonstrated [16]. Nevertheless, these assumptions and approximations limit our ability to describe accurately and characterize chromatic dispersion at all the frequencies that are important for dynamics of optical devices using DDE models. Another approach is to investigate rigorously derived DDEs where higher order dispersion arises naturally (e.g., coupled cavities [17]), however quantification of its magnitude for a given DDE is not a trivial task.

In this paper, we consider an externally injected ring Kerr cavity with two linear spectral filters introducing an effective chromatic dispersion and demonstrate the possibility to model arbitrary second-order dispersion near a chosen frequency within the DDE approach framework. We develop a second order DDE model of the system under consideration and demonstrate the appearance of MI and the formation of bright localized structures in this model in the anomalous dispersion regime. The system under consideration can be realized experimentally to generate temporal cavity solitons and the corresponding optical frequency combs [18, 19]. We show that in a certain limit our model can be reduced

DOI 10.20347/WIAS.PREPRINT.2948 Berlin 2022

to a generalized version of the well-known Lugiato-Lefever equation [20], which is widely used to describe optical microcomb generation [21, 22, 23], with an additional diffusion term. These results can be applied to qualitatively analyze any optical set-up that can be modeled using delay equations such as Fourier domain mode-locked [15], optically injected [16], and multisection mode-locked semiconductor lasers as well as any other system, where second-order chromatic dispersion is important (see references in [15]). We note also that two spectral filters with different central frequencies are used in Mamyshev oscillators, which employ active cavity to generate short optical pulses. Hence this work not only presents the simplest dispersive second-order DDE model that can describe complicated phenomena like localized structures, but also could provide better understanding of the effect of two filters in the cavity and a basis for the theoretical investigation of Mamyshev oscillators [24, 25].

# 2 Model equations

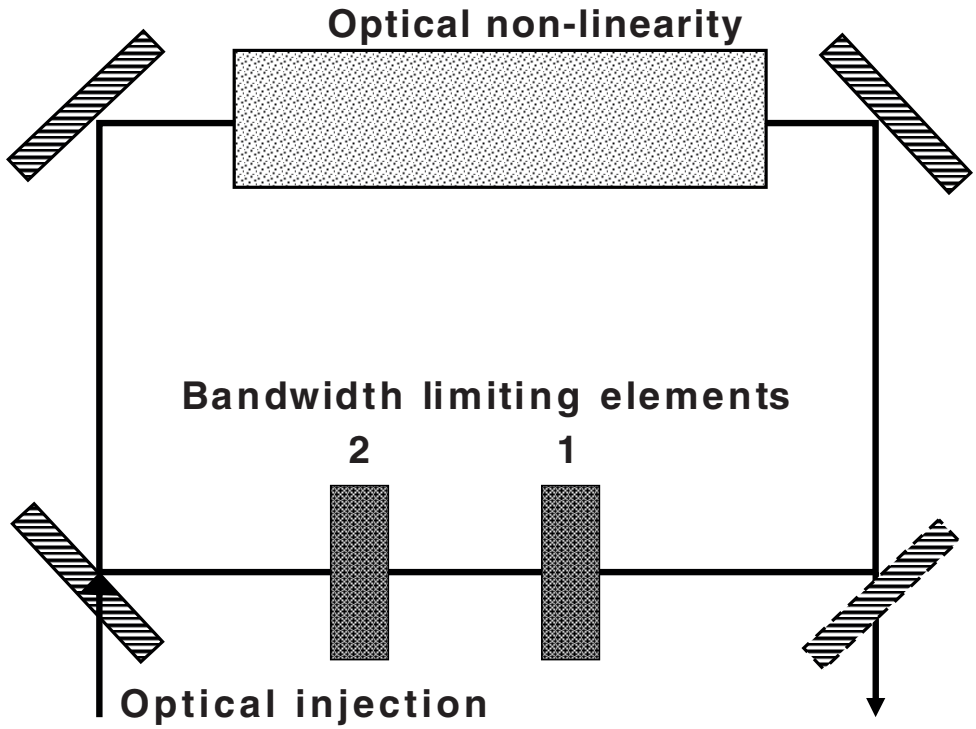


Figure 1: Schematic representation of the considered device

## 2.1 DDE model

We consider an optically injected passive nonlinear cavity with two linear Lorentzian filters inside it (see Fig. 1). For this system using the lumped element method described in [3, 4, 5] we obtain the following set of delay differential equations

$$B'(t) + (\gamma_1 - i\omega_1)B(t) = \gamma_1\gamma_2\left[\sqrt{\kappa_l}e^{i\alpha|A(t-T)|^2+i\phi}A(t-T) + \eta_0 e^{i\omega_0 t}\right], \tag{1}$$

$$A'(t) + (\gamma_2 - i\omega_2)A(t) = B(t), \tag{2}$$

where $B$ and $A$ represent electrical field envelopes after the first and the second filter, respectively, $T$ is the cavity round-trip time, $\kappa_l$ is the intensity attenuation factor due to the linear cavity losses, $\varphi$

is the phase shift, $\alpha$ is the Kerr coefficient which, without the loss of generality can be assumed to be positive, $\eta_0$ and $\omega_0$ are the injection rate and frequency offset, $\omega_1$ and $\omega_2$ are the central frequencies of the two filters, while $\gamma_1$ and $\gamma_2$ are their bandwidths. The system (1) and (2) can be considered as an extension of the Ikeda map [1], which takes into consideration the spectral filtering introduced by two Lorentzian filters.

## 2.2 Transfer function of the filter

The transfer function of the two filters shown in Fig. 1 can be written in the standard form [14, 15]

$$F(\omega) = e^{f(\omega)}, \tag{3}$$

where the complex function $f(\omega)$ can be expanded in power series near $\omega = 0$

$$f(\omega) = \sum_k D_k \omega^k, \tag{4}$$

and $\operatorname{Im} D_k$ represents the dispersion of the $k$th order. [1]

From Eqs. (1) and (2) one obtains that the two filter transfer function is

$$F(\omega) = \frac{\gamma_1\gamma_2}{[\gamma_1 + i(\omega - \omega_1)]\,[\gamma_2 + i(\omega - \omega_2)]}. \tag{5}$$

Without the loss of generality we can assume that $\gamma_1 \geq \gamma_2$ and the reference frequency is chosen in such a way that the maximum of the function $|F(\omega)|$ is at $\omega = 0$, so that $\left[\frac{d|F(\omega)|}{d\omega}\right]_{\omega=0} = 0$. The latter condition is equivalent to

$$\delta_F = \gamma_2^2\omega_1 + \omega_2\left[\gamma_1^2 + \omega_1(\omega_1 + \omega_2)\right] = 0, \tag{6}$$

which has two solutions $\omega_2 = \omega_{2\pm} = \frac{-\gamma_1^2 - \omega_1^2 \pm \sqrt{D_F}}{2\omega_1}$, $D_F = -4\gamma_2^2\omega_1^2 + (\gamma_1^2 + \omega_1^2)^2$. One can see that both $\omega_{2\pm}$ can be obtained for any values of $\omega_1 \neq 0$ and $0 < \gamma_2 < \gamma_1$ due to $D_F > 0$, and, moreover,

$$|\omega_1^2 - \gamma_1^2| \leq \sqrt{D_F} \leq \gamma_1^2 + \omega_1^2.$$

Below we will assume that the condition $\omega_2 = \omega_{2+}$ is satisfied that corresponds to a situation when the largest of the two maximums of $|F(\omega)|$ is located at zero frequency (see Fig. 2). Moreover, for $\omega_2 = \omega_{2+}$ we have

$$\omega_2\omega_1 < 0, \quad |\omega_2| \leq |\omega_1|, \quad \left|\frac{d\omega_2}{d\omega_1}\right| < 1,$$

and one can see that

$$\frac{d|\omega_2 - \omega_1|}{d|\omega_1|} > 0,$$

i.e. the difference between the two frequencies grows with $|\omega_1|$, and since for any of $\omega_1 = \pm\omega_1^*$ we have $\omega_2 = \mp\omega_2^*$, respectively, for any fixed $0 < \gamma_2 < \gamma_1$ we can choose $|\omega_2 - \omega_1|$ and find

[1] For example, for a single Lorentzian absorption line we have $f = \frac{-\sigma L}{\Gamma + i(\omega + \Omega)}$ [15], and second-order dispersion coefficient takes the form $\operatorname{Im} D_2 = \operatorname{Im} \frac{d^2 f}{d\omega^2} \approx \frac{2\sigma L}{\Omega^3}$ for $0 < \Gamma \ll |\Omega|$, and the sign of the coefficient coincides with the sign of $\Omega$.

corresponding value of $\omega_1$ (negative or positive) and $\omega_2 = \omega_{2+}$, which means that we can have any possible combinations of two filters (narrow filter to the left or to the right of the broad filter), disregarding frequency shift of the combined filter. Moreover, these inequalities immediately imply that the largest maximum of $|F(\omega)|$ is at $\omega = 0$ for $\omega_2 = \omega_{2+}$ as claimed earlier, since more narrow Lorentzian filter with the width $\gamma_2$ has the central frequency $\omega_2$ closer to zero frequency. The other root (6) $\omega_2 = \omega_{2-}$ can correspond to a global maximum, a local maximum, or a local minimum, which do not provide any additional useful alternatives, if we are interested to fix the maximum of the combined filter $|F(\omega)|$ at zero frequency $\omega = 0$.

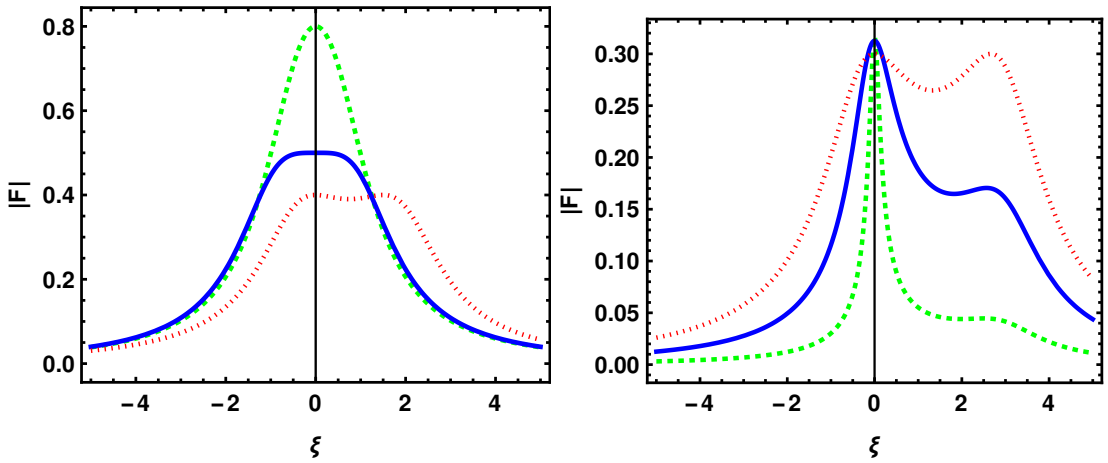


Figure 2: Absolute value of the transfer function $F$ defined by Eq. (5), where $\omega_2 = \omega_{2+}$ satisfies (6), $\gamma_1 = 1$ and other parameters are varied: (left) $\gamma_2 = 1$, $\omega_1 = \frac{1}{2}$ (dashed), $\omega_1 = 1$ (solid), $\omega_1 = 2$ (dotted); (right) $\omega_1 = 3$, $\gamma_2 = \frac{1}{8}$ (dashed), $\gamma_2 = \frac{1}{2}$ (solid), $\gamma_2 = 1$ (dotted). The corresponding values of $\omega_2$, $\beta$, $\sigma$ are $\{-\frac{1}{2}, -1, -\frac{1}{2}\}$, $\{0, 0, \frac{3}{4}\}$ and $\{\frac{4}{\sqrt{5}}, \sqrt{2}, \frac{5}{\sqrt{8}}\}$ (left); $\{-0.0047, -0.07677, -\frac{1}{3}\}$, $\{2.66, 1.95, \frac{4}{3}\}$ and $\{8.58, 3.84, \frac{5\sqrt{2}}{3}\}$ (right).

Since $f(\omega) = \ln F(\omega)$, in the power series expansion (4) we obtain the second-order coefficient as

$$D_2 = \frac{\omega_1^2 - \gamma_1^2 - 2i\gamma_1\omega_1}{2(\gamma_1^2 + \omega_1^2)^2} + \frac{\omega_2^2 - \gamma_2^2 - 2i\gamma_2\omega_2}{2(\gamma_2^2 + \omega_2^2)^2}.$$

One can check that $D_2$ can be represented in the following way

$$D_2 = \rho\left(-\frac{\sigma^2 - 2}{2} + i\beta\right) + \frac{\delta_F\left[\delta_F - 2i\left(\gamma_1^2\gamma_2 + \gamma_1\gamma_2^2 + \gamma_2\omega_1^2 + \gamma_1\omega_2^2\right)\right]}{2\left(\gamma_1^2 + \omega_1^2\right)\left(\gamma_2^2 + \omega_2^2\right)\left(\gamma_1\gamma_2 - \omega_1\omega_2\right)}, \tag{7}$$

with

$$\rho = \frac{\gamma_1\gamma_2 - \omega_1\omega_2}{\left(\gamma_1^2 + \omega_1^2\right)\left(\gamma_2^2 + \omega_2^2\right)}, \tag{8}$$

$$\sigma = \frac{\sqrt{\rho}\left(\gamma_1^2\gamma_2 + \gamma_1\gamma_2^2 + \gamma_2\omega_1^2 + \gamma_1\omega_2^2\right)}{\gamma_1\gamma_2 - \omega_1\omega_2}, \tag{9}$$

$$\beta = \frac{\gamma_1\omega_2 + \gamma_2\omega_1}{\gamma_1\gamma_2 - \omega_1\omega_2}. \tag{10}$$

It follows from the conditions (6), where $\omega_2 = \omega_{2+}$, and the relation $\gamma_1 \geq \gamma_2$ that the second term in the right hand side (RHS) of (7) vanishes, $\rho > 0$, and sign$\beta$ = sign$\omega_1$. Hence, the parameters $\beta$ and $\frac{\sigma^2-2}{2}$ represent the normalized second-order dispersion and the diffusion near zero frequency, respectively, whereas the parameter $\sqrt{\rho}$ can be considered as a scaling coefficient.

One can see that under these conditions

$$\frac{d|\beta|}{d|\omega_1|} > \frac{\sqrt{D}(\sqrt{D}+\omega_1^2-\gamma_1^2)}{4\gamma_1\omega_1^2(\gamma_1^2+\omega_1^2)} > 0,$$

and since $|\omega_2-\omega_1|$ grows with $|\omega_1|$, second-order dispersion grows with the difference between the frequencies. Moreover, using (6) to express $\omega_2^2$ one obtains

$$\sigma = \frac{(\gamma_2\omega_1-\gamma_1\omega_2)\text{Sign}\,\omega_1}{\sqrt{\omega_1\omega_2(\omega_1\omega_2-\gamma_1\gamma_2)}},$$
$$\frac{d\sigma}{d\gamma_2} = \frac{|\omega_1|(\gamma_1\gamma_2\omega_1+(\gamma_1^2-2\omega_1^2)\omega_2)(\gamma_2\frac{d\omega_2}{d\gamma_2}-\omega_2)}{2(\omega_1\omega_2(\omega_1\omega_2-\gamma_1\gamma_2))^{3/2}},$$
$$\gamma_2\frac{d\omega_2}{d\gamma_2}-\omega_2 = \omega_2\frac{\gamma_1^2+\omega_1^2}{2\sqrt{D}},$$
$$\omega_1(\gamma_1\gamma_2\omega_1+(\gamma_1^2-2\omega_1^2)\omega_2) < -\frac{\gamma_1^2(\gamma_1^2+\omega_1^2)}{2},$$

hence due to $\omega_1\omega_2 < 0$ we see that $\frac{d\sigma}{d\gamma_2} < 0$, and $\sigma$ decreases with $\gamma_2$ increasing from 0 to $\gamma_1$. Therefore, the lower bound on $\sigma$ can be estimated assuming $\gamma_2=\gamma_1$, where $\omega_2 = \frac{-\gamma_1^2-\omega_1^2+|\omega_1^2-\gamma_1^2|}{2\omega_1}$ and

$$\sigma \geq \sigma_{\gamma_2=\gamma_1} = \begin{cases} \sqrt{2}\sqrt{1+\beta^2}, |\omega_1| \geq \gamma_1, \\ 2\frac{\gamma_1\sqrt{1+\beta^2}}{\sqrt{\gamma_1^2+\omega_1^2}}, |\omega_1| < \gamma_1. \end{cases} \geq \sqrt{2}\sqrt{1+\beta^2}. \tag{11}$$

## 2.3 Normalized DDE model

By substituting Eq. (2) into Eq. (1), using Eq. (6), and rescaling time as $t \to t/\sqrt{\rho}$, we obtain the following normalized dimensionless second-order DDE

$$A''(t)(1+i\beta)+\sigma A'(t)+A(t) = \sqrt{\kappa}e^{i\alpha|A(t-T)|^2+i\varphi}A(t-T)+\eta e^{i\omega_0 t}, \tag{12}$$
$$\sigma > \sqrt{2}\sqrt{1+\beta^2},$$

where losses and forcing take the form $\sqrt{\kappa}=r\sqrt{\kappa_l}\leq 1$, $\eta = r\eta_0$ with $r=\frac{\gamma_1\gamma_2}{\sqrt{(\gamma_1^2+\omega_1^2)(\gamma_2^2+\omega_2^2)}}\leq 1$, and the phase shift is $\varphi=\phi+\arg\frac{1}{\gamma_2\gamma_2-\omega_1\omega_2-i(\gamma_1\omega_2+\omega_2\gamma_1)}$. Here, similarly to the previous section one can see that $\frac{dr}{d|\omega_1|}<0$ for $\gamma_1>\gamma_2$ and $\omega_2=\omega_{2+}$, hence for fixed $\kappa_l$ the parameter $\kappa$ decreases with increasing detuning between the two frequencies $|\omega_2-\omega_1|$. With the condition (11) on dimensionless parameters $\sigma$ and $\beta$ the equation is equivalent to the system with two filters (1)-(2) for any $\kappa<1$ with global maximum of the combined filter transfer function $F(\omega)$ (5) located at zero frequency $\omega=0$, $|F(\omega)|\leq|F(0)|\leq 1$. We note that for $\sqrt{2}\leq\sigma\leq\sqrt{2(1+\beta^2)}$ the global maximum of $F(\omega)$ is at another frequency and additional constraints on parameter $\kappa$ are necessary, whereas for $\sigma<\sqrt{2}$ the diffusion coefficient in (7) becomes negative, equivalence with (1)-(2) is lost and zero solution $A=0$ for $\eta=0$ is unstable.

For $\beta=0$ relation (7) gives zero dispersion coefficient and diffusion coefficient equal to $(\sigma^2-2)/2$, which agrees with previous analysis of a similar DDE [26] in case of $\sigma>\sqrt{2}$.

We note that the direct application of truncated expansion (4) in the RHS of DDE models similar to (1) and (12) would lead to the appearance of the second derivative of the delayed variable $A''(t-T)$ in

and spurious instability [15]. In contrast, non-delayed second order derivative $A''(t)$ in (12) appears without any expansions, and the term $i\beta A''(t)$ is responsible for the second-order chromatic dispersion similarly to the NLS equation. On the other hand, unlike the cubic CGL model, where the real coefficient by the second derivative is responsible for the diffusion (or parabolic spectral filtering), the filtering in (12) is performed by two Lorentzian filters, which are introduced by the presence of of both the first and the second order derivatives. Therefore, the generality of this kind of dispersion operator is still not directly comparable to the operators in NLS-type equations or systems with distributed delay [15]. However, in contrast to the approximate DDEs [16], the physical meaning of this filter is clear for any feasible parameters. For simplicity below we consider the case of non-detuned injection, $\omega_0 = 0$.

### 2.4 Limit of Lugiato-Lefever equation

Assuming large delay limit $T = r/\varepsilon$, where $\varepsilon \ll 1$ and $r = 1 + a_1\varepsilon + a_2\varepsilon^2 + \ldots$, taking $\omega_0 = 0$, and rescaling the time variable $t \to t/\varepsilon$ we can rewrite (12) in the form

$$\varepsilon^2 A''(t)(1 + i\beta) + \varepsilon\sigma A'(t) + A(t) = \sqrt{\kappa}e^{i\alpha|A(t-r)|^2+i\varphi}A(t-r) + \eta, \tag{13}$$

Let the injection rate, the linear cavity losses and the phase shift be small,

$$\eta = \varepsilon^3 S, \quad \kappa = 1 - 2\varepsilon^2 k, \quad \varphi = \varepsilon^2\theta. \tag{14}$$

Then looking the solution in the form $A(t) = \varepsilon u(t,\tau) + \varepsilon^2 v(t,\tau) + \ldots$ with $\tau = \varepsilon^2 t$, applying multiscale analysis [27, 28], and collecting the first order in $\epsilon$ and using solvability condition of the the resulting equation we get the periodic boundary condition:

$$u(t,\tau) = u(t-1,\tau). \tag{15}$$

Next, in the second order in $\varepsilon$ we obtain

$$v(t,\tau) - v(t-1,\tau) = a_1 u_t(t-1,\tau) - \sigma u_t(t,\tau),$$

which impl the periodicity of $v$, $v(t-1,\tau) = v(t,\tau)$ and the relation $a_1 = \sigma$ with the periodicity condition (15). Finally collecting the third order terms in $\varepsilon$, using the relation $a_2 = \sigma^2$, and applying solvability condition [27, 28] we get the generalized Lugiato-Lefever equation (LLE)

$$u_\tau = S - ku + i\theta u + i\alpha u|u|^2 + \left(\frac{\sigma^2 - 2}{2} - i\beta\right) u_{tt} \tag{16}$$

with the diffusion coefficient $(\sigma^2 - 2)/2$ the boundary condition (15). It is well known that for the condition $\beta < 0$ in Eq. (16) corresponds to anomalous dispersion regime, and for $\theta < 0$ this equation can demonstrate the formation of bright dissipative solitons [20]. Dimensionless dispersion and diffusion coefficients in Eq. (16) coincide with those defined by Eq. (7).

## 3 Continuous wave (CW) state

The CW state of the equation (12) with $\omega_0 = 0$ takes the form $A = A_0 e^{i\psi}$, where the real quantities $A_0$ and $\psi$ satisfy the system of the transcendental equations

$$A_0\left[1 - \sqrt{\kappa}\cos\left(\alpha A_0^2 + \varphi\right)\right] = \eta\cos\psi, \tag{17}$$

$$A_0\sqrt{\kappa}\sin\left(\alpha A_0^2 + \varphi\right) = \eta\sin\psi, \tag{18}$$

which leads to a single transcendental equation for $A_0^2$

$$A_0^2\left[\kappa+1-2\sqrt{\kappa}\cos\left(\alpha A_0^2+\varphi\right)\right]=\eta^2. \tag{19}$$

Assuming $\varepsilon \ll 1$, $A_0=\varepsilon u_0$, $\varphi=\varepsilon^2\theta$, $0<1-\kappa\sim 2\varepsilon^2 k$, and $\eta=\varepsilon^3 S$, this equation can be approximated by a cubic equation for $u_0^2$

$$S^2\approx u_0^2\left[k^2+(\theta+\alpha u_0^2)^2\right], \tag{20}$$

which coincides with the equation for the uniform stationary solutions of the LLE (16). Therefore, in this limit equation (12) can have up to three coexisting CW states similarly to LLE (see Fig. 3, left), however out of this limit for strong injection there can be more coexisting CW states, see right panel of Fig. 3. Here, the upper CW state looses stability via a modulational instability, and unstable CW states are shown by dotted red line.

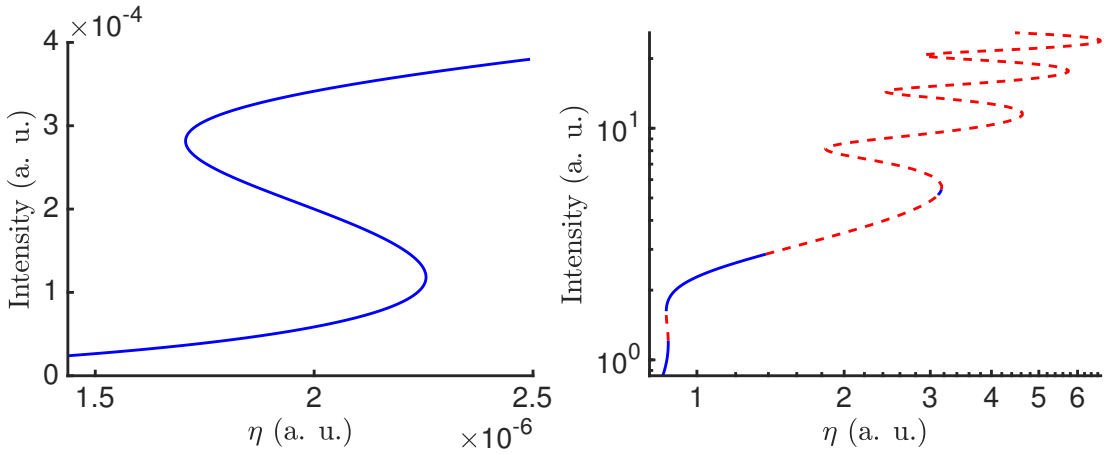


Figure 3: Intensity $|A_0|^2$ of CW states (17)-(18) obtained by varying parameter $\eta$ (left). Here, $\omega_0=0$, $\kappa=1-10^{-4}, \sigma=\sqrt{2.5}, \alpha=1, \varphi=-3\times10^{-4}$, which in the LLE limit (13) corresponds to $\varepsilon=0.01$, see Fig. 6. In the right panel we choose $\kappa=\exp(-2), \varphi=-2$, which corresponds to $\varepsilon=1$, where solid lines correspond to stable CWs and dashed - to unstable.

## 3.1 Stability of CW solution and MI

Here, we demonstrate how MI of an initially stable CW state can appear in the anomalous dispersion regime in the limit of large delay $T\gg 1$. For that, we linearize the equation (12) near the CW state $A(t)=(A_0+\delta A e^{\lambda t})e^{i\psi}$ and calculate the determinant of the Jacobian of the linearised system to obtain the following characteristic equation for the eigenvalues $\lambda$ describing the stability of the CW solution:

$$\begin{aligned}\kappa Y^2+\lambda\{\lambda\left[\left(\beta^2+1\right)\lambda^2+2\lambda\sigma+\sigma^2+2\right]+2\sigma\}+1+\\ 2\sqrt{\kappa}Y\{\sin\left(\alpha A_0^2+\varphi\right)\left[\alpha A_0^2\left(\lambda^2+\lambda\sigma+1\right)-\beta\lambda^2\right]-\\ \cos\left(\alpha A_0^2+\varphi\right)\left[\lambda^2\left(\alpha A_0^2\beta+1\right)+\lambda\sigma+1\right]\}=0.\end{aligned} \tag{21}$$

where $Y(\lambda)=\exp(-\lambda T)$. In the limit of large delay time $T\to\infty$ the eigenvalues belonging to the pseudo-continuous spectrum can be represented in the form $\lambda=i\mu+\frac{\Lambda}{T}+\mathcal{O}(1/T^2)$ with real $\mu$ [29].

Thus, in this limit the characteristic equation is a quadratic equation for $Y$ with the coefficients depending only on the imaginary part $\mu$ of the eigenvalue, and we can obtain from (21) two branches of pseudo-continuous spectrum given by

$$\Lambda_{\pm}(\mu) = -\operatorname{Re}\ln Y_{\pm}(i\mu). \tag{22}$$

For a stable CW solution we have $\Lambda_{\pm}(\mu) \leq 0$ and, in particular, $\Lambda_{\pm}(0) = -\operatorname{Re}\ln Y_{\pm}(0) \leq 0$, where

$$Y_{\pm}(0) = \frac{1}{\sqrt{\kappa}}\left[\cos\left(\alpha A_0^2+\varphi\right) - \alpha A_0^2 \sin\left(\alpha A_0^2+\varphi\right) \pm \sqrt{D}\right], \tag{23}$$

$$D = \left[\cos\left(\alpha A_0^2+\varphi\right) - \alpha A_0^2 \sin\left(\alpha A_0^2+\varphi\right)\right]^2 - 1. \tag{24}$$

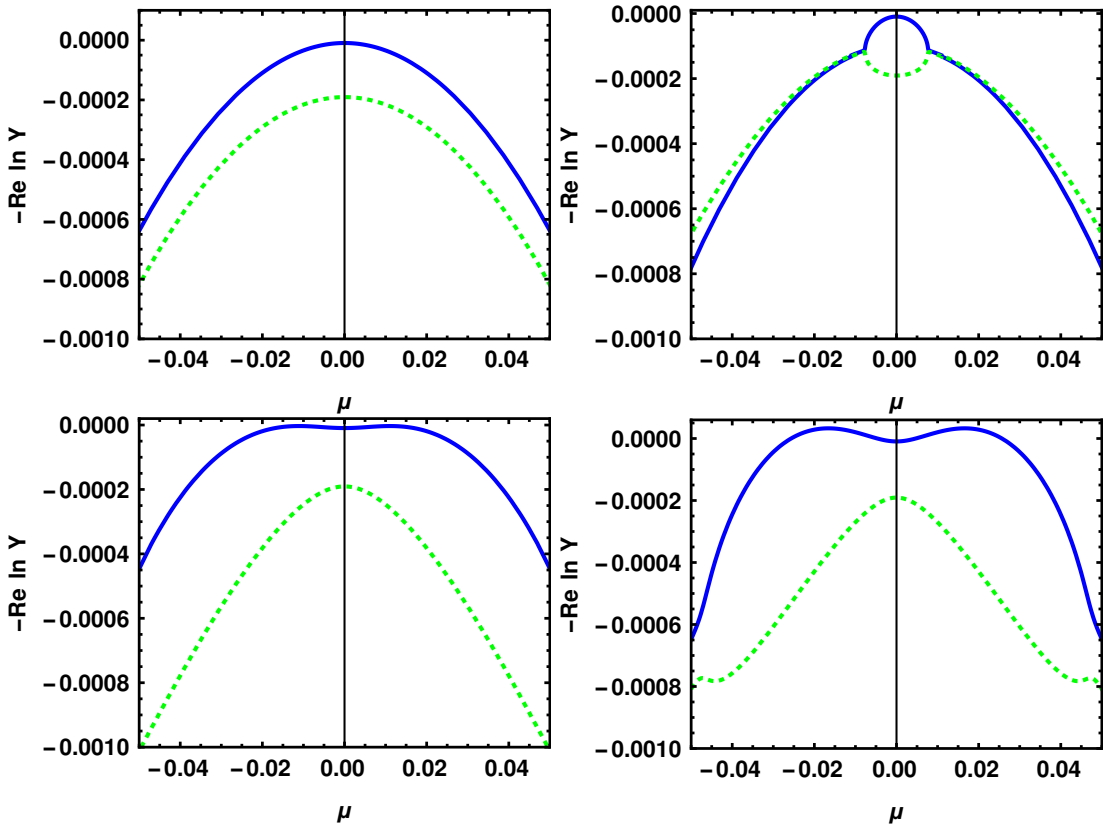


Figure 4: Curves of pseudocontinuous spectrum in the limit of large delay (21) of (12) of the CW with the largest intensity ($|A_0| \approx 0.0169$ out of another two $|A_0| \approx 0.0167$ and $|A_0| \approx 0.006$) near the LLE limit, $\eta \approx 1.707 \times 10^{-6}$, and varying $\beta = 0$ (top-left), $\beta = 1/4$ (top-right), $\beta = -1/8$ (bottom-left), $\beta = -1/4$ (bottom-right). Other parameters are as in Fig. 3

.

Moreover, the second derivative of $\Lambda_{\pm}(\mu)$ at $\mu = 0$ takes the form

$$\Lambda''_{\pm}(0) = 2 - \sigma^2 \pm 2\beta \operatorname{Re}\mathcal{B}(\alpha,\varphi,\eta,\kappa), \tag{25}$$

$$\mathcal{B} = \frac{\alpha A_0^2 \cos\left(\alpha A_0^2+\varphi\right) + \sin\left(\alpha A_0^2+\varphi\right)}{\sqrt{D}}. \tag{26}$$

One can see from (25) that for small $\beta \approx 0$ and $\sigma > \sqrt{2}$ we have $\Lambda''_{\pm}(0) < 0$ for the CW solutions on the upper branch of S-shaped bifurcation curve depicted in Fig. 3 (see top-left panel of Fig. 4). It

is known that strong anomalous dispersion can lead to the change of the curvature of one of the two branches $\Lambda_{\pm}(\mu)$ of the pseudo-continuous spectrum at $\mu = 0$ (see Fig. 4, bottom-left) [15]. Moreover, further increase of anomalous dispersion can lead to a MI of a CW state (see Fig. 4, bottom-right) [16]. On the other hand, in the case of strong normal dispersion regime the sign change of the curvature of the curve with smaller $\Lambda_{\pm}(0)$ does not lead to a MI, as it is seen from the top-right panel of Fig. 4.

The stability condition of the CW state can be written in the form $|Y_{\pm}(i\mu)| > 1$ for all the wavenumbers $\mu$. In particular, at zero wavenumber $\mu = 0$ we get

$$|Y_{\pm}(0)| > 1. \tag{27}$$

A CW solution satisfying this condition is stable with respect to perturbations at zero wavenumber, but may be unstable with respect to MI at nonzero wavenumbers. A possible (but not unique) way how such a MI can develop is related to the change of the sign from negative to positive of one of the two quantities $\Lambda''_{\pm}(0)$ corresponding to the greater of the two values $\Lambda''_{\pm}(0)$. Note, that both the quantities $\Lambda''_{\pm}(0)$ are always negative at $\beta = 0$ due to the inequality (11). It follows from Eq. (26) that such a sign change can take place only in the case when

$$D > 0 \tag{28}$$

and, hence, $Y_{\pm}(0)$ must be real. Otherwise, $\mathcal{B}$ is purely imaginary and the last term in the RHS of Eq. (25) vanishes. It is shown in Appendix A that in the LLE limit (14) we have $\Lambda_{+}(0) < \Lambda_{-}(0)$ and for the CW state with the highest intensity we can have $\Lambda''_{-}(0) > 0$ only in the anomalous dispersion regime $\beta < 0$ . Out of LLE limit we can have positive $\Lambda''_{\pm}(0)$ in case of $\beta > 0$ as well (see Appendix B for numerical treatment).

Note, that the development of MI on the stable upper part of the CW branch can be correlated with the appearance of stable localized structures. In the next section we study numerically how the dispersion coefficient $\beta$ affects the existence range of these structures. Remarkably, there are also scenarios out of the LLE limit where localized structures can be observed for zero and small positive $\beta$.

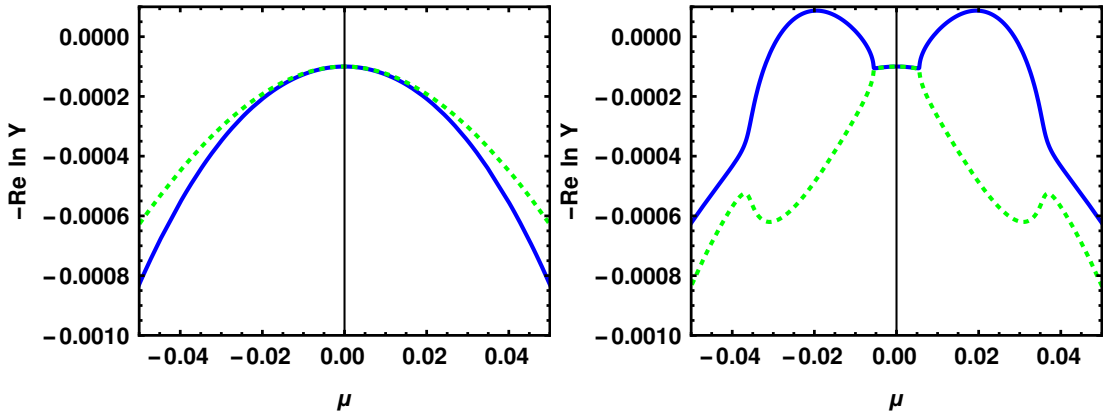


Figure 5: Curves of pseudocontinuous spectrum in the limit of large delay (21) of (12) of the CW with the largest intensity ($|A_0| \approx 0.0178$ out of another two $|A_0| \approx 0.0156$ and $|A_0| \approx 0.0065$) near the LLE limit with $\beta = 1/2$ (left) and $\beta = 1/2$ (right), and $\eta \approx 1.797 \times 10^{-6}$. Other parameters are as in Fig. 3

.

We note that the condition $\Lambda''(0) > 0$ precedes the appearance of MI of the CW for stronger dispersion if $Y_{\pm}(0)$ is real-valued. If it's complex-valued, MI is still possible for sufficiently strong dispersion

(see Fig. 5). In the LLE limit, one can derive an approximate condition for MI development (see Appendix), and demonstrate that for typical parameters in this limit strong anomalous dispersion can lead to the instability.

# 4 Numerical results

In this section, we perform numerical bifurcation analysis of equation (12) using DDE-BIFTOOL [30]. Let us start with the parameter set close to the LLE limit. We take $\sigma = \sqrt{2.5}$, $\beta = -0.5$, which corresponds to two filters (5) with $\gamma_1 = \gamma_2, \omega_1 = -\frac{1+\sqrt{5}}{2}\gamma_1 \approx -1.62\gamma_1, \omega_2 = \frac{\sqrt{5}-1}{2}\gamma_2 \approx 0.62\gamma_2$.Let $\alpha = 1, \omega_0 = 0$ and $\varphi = \varphi_\varepsilon, \kappa = \kappa_\varepsilon$, where

$$\kappa_\varepsilon = \exp(-2\varepsilon^2), \quad \varphi_\varepsilon = -2\varepsilon^2$$

are chosen according to analysis of DDE (13) in the limit $\varepsilon \to 0$. These values directly correspond to the parameters of LLE (16) where localized structures are known to exist ($\theta = \varphi/\varepsilon^2 < -\sqrt{3}$). We also pick a reference injection strength

$$\eta_\varepsilon = \varepsilon^3 \sqrt{\frac{8}{\sqrt{3}^3} + \frac{4}{3}\left(-\frac{\varphi_\varepsilon}{\varepsilon^2} - \sqrt{3}\right)}, \tag{29}$$

where three CW states are guaranteed to coexist for $\varepsilon \ll 1$, and vary $\eta$ near $\eta_\varepsilon$. The main numerical difficulty in this limit is that the delay time $T$ and the width of the localized structures are proportional to the large quantity $\varepsilon^{-1}$. Figure 6 was obtained with $\varepsilon = 0.05$, which was the smallest value of $\varepsilon$ used in our simulations and corresponded to $\kappa \approx 0.995$. Similarly to the LLE [31, 32] the bifurcation diagram in the left panel of this figure shows a typical S-shaped CW branch with stable lower part and modulationally unstable upper part. The branch of unstable periodic solutions bifurcates from the unstable middle part of the CW branch and it becomes stable after a fold bifurcation at $\eta \approx 0.00022$. The stable periodic solution has only a slight asymmetry in its time profile and resembles the temporal dissipative solitons of the LLE, see right panel of Fig. 6.

Thus, close to the limit $\varepsilon \to 0$ the normalized second-order DDE (12) demonstrates the bifurcation structure similar to that of the LLE. Note, however, that the magnitude of the parameters $\sigma$, $\beta$ and $1 - \kappa$ in the normalized equation (12) depends on the frequency detuning of the linear filters with respect to each other in the original equivalent system (1)-(2), and stronger detuning results for fixed $\sigma$ in larger $|\beta|$ as discussed in Section 2.2, and higher losses $1 - \kappa$ at the same time as discussed in Section 2.3. Therefore, it is necessary to investigate how larger values of $\varepsilon$ corresponding to smaller values of the attenuation factor $\kappa$ (larger losses) affect the properties of the localized solutions. For example, for the considered parameters $\sigma = \sqrt{2.5}$ and $\beta = -0.5$ from Eqs. (1)-(2) and the condition $\kappa_l \leq 1$ one obtains $\kappa \leq 0.4$ in (12), which is satisfied for $\varepsilon \geq 0.7$.

For larger $\varepsilon = 0.2$, which corresponds to $\kappa \approx 0.92$, the stable part of the periodic solution branch is split into two parts separated by two fold bifurcation points, see left panel of Fig. 7. Both these parts correspond to very asymmetric localized pulses, but the second part contains wider pulses then the first one, see right panel of Fig 7. Figures 8 and 9 show the branches of CW and periodic solutions with scaled intensity [2] obtained by increasing gradually $\varepsilon$ up to $1$, which corresponds to $\kappa \approx 0.135$.

[2] In these figures $\eta$ is shifted, more precisely, $\tilde{\eta} = \eta - \eta_\varepsilon - \eta_{1,j} + 10^{-5} j$ for the left panel of Fig. 8, $\tilde{\eta} = \eta - \eta_\varepsilon - \eta_{2,j} + 5j\eta_{2,1}$ for the right panel, $\tilde{\eta} = \eta - \eta_\varepsilon - \eta_{1,j} + 10^{-2}(j-4)$ for the left panel of Fig. 9, $\tilde{\eta} = \eta - \eta_\varepsilon - \eta_{2,j} + 2\times 10^{-3}(j-4)$ for the right panel, and $\varepsilon = \epsilon_j$, $\vec{\epsilon} = \{0.05, 0.1, 0.2, 0.3, 0.4, 0.5, 0.6, 0.7, 0.8, 0.9, 1.0\}$, $\vec{\eta}_1 = \{-1.2 \times 10^{-5}, -1.634 \times 10^{-4}, -7.69 \times 10^{-4}, -0.0039, -0.0136, -0.0245, -0.059, -0.11, -0.195, -0.347, -0.5474\}$, $\vec{\eta}_2 = \{1.413 \times 10^{-6}, 4.3 \times 10^{-6}, -1.2 \times 10^{-4}, -0.0015, -0.006, -0.019, -0.047, -0.099, -0.185, -0.333, -0.5294\}$

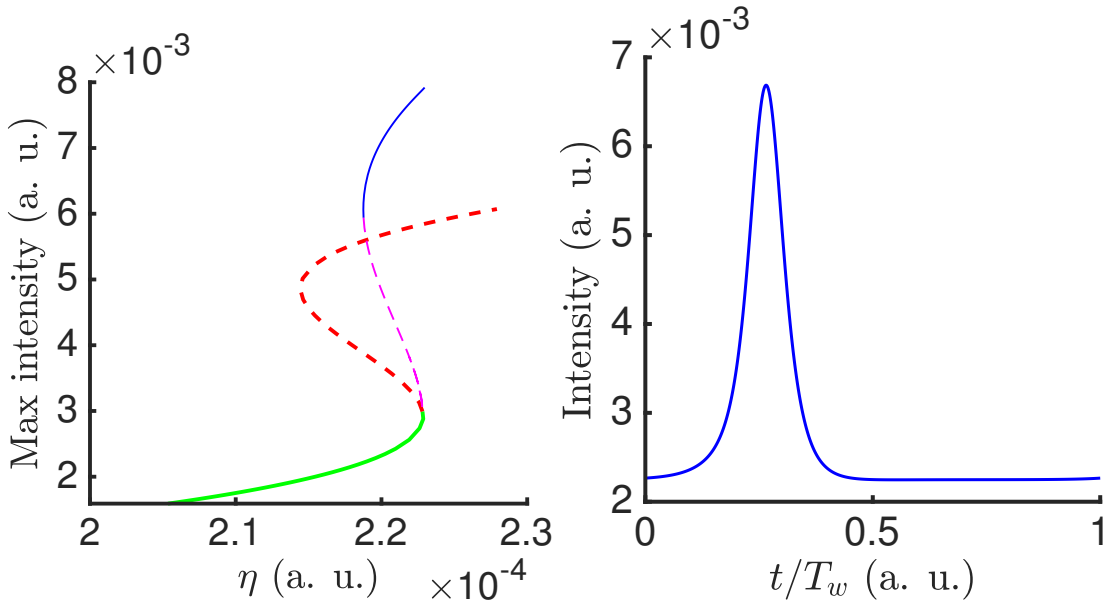


Figure 6: Left panel: One-parameter bifurcation diagram of Eq. (12) with $\varphi = \varphi_\varepsilon$, $\kappa = \kappa_\varepsilon$, and $\varepsilon = 0.05$. CW (periodic) solutions are shown by thick (thin) lines. Solid lines represent stable states and dashed lines represent unstable states. The parameter $\eta$ is changed near $\eta_\varepsilon$ defined by Eq. (29). Right panel: Stable localized periodic solution for $\eta \approx 0.000223$, where $T_w \sim 1/\varepsilon$ is the period of the solution controlled by the choice of delay time $T$. Other parameters are $\alpha = 1, \sigma = \sqrt{2.5}, \beta = -0.5$.

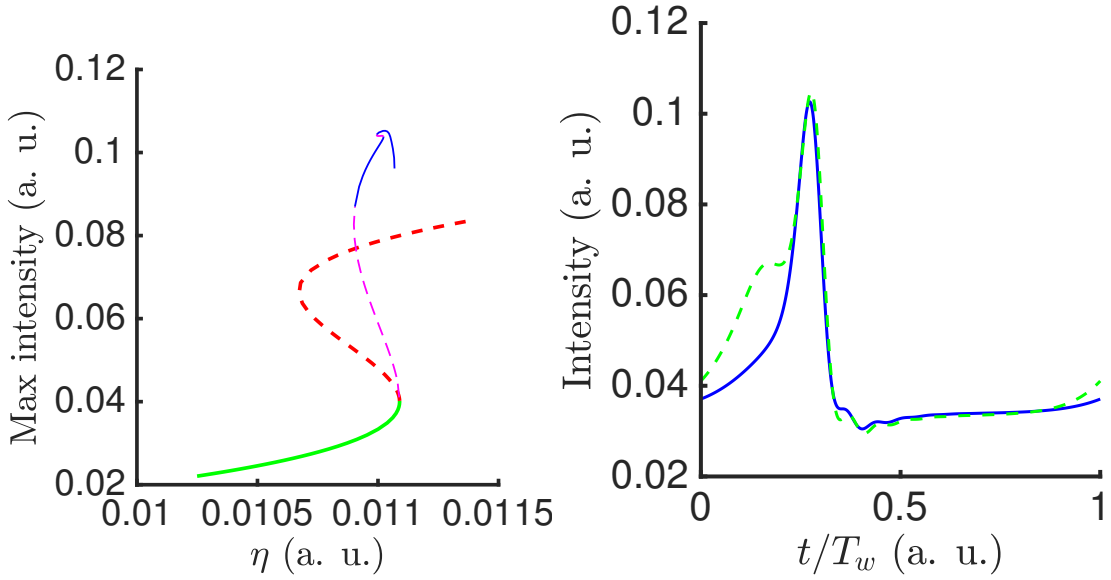


Figure 7: Left panel: One-parameter bifurcation diagram of Eq. (12) with $\varphi = \varphi_\varepsilon$, $\kappa = \kappa_\varepsilon$, and $\varepsilon = 0.2$. CW (periodic) solutions are shown by thick (thin) lines. Solid lines represent stable states and dashed lines represent unstable states. The parameter $\eta$ is changed near $\eta_\varepsilon$ defined by Eq. (29). Right panel: Stable localized periodic solutions for the same $\eta$ from the first (main) stable part of the periodic solution branch (solid) and the secondary stable part (dashed). Other parameters are as in Fig. 6.

The width of the S-shaped area of the CW branches as well as the width of the branch of the localized solutions increases with $\varepsilon$ up to $\varepsilon = 0.8$ and then decreases. For $\varepsilon \geq 0.4$ the upper branch of CW states stabilizes for the chosen parameter values (Fig. 9, left). Asymmetric localized structures

corresponding to the stable parts of the periodic solution branches with $\varepsilon \geq 0.2$ in Fig. 10 look similar to the those shown in the right panel of Fig. 7 obtained for $\varepsilon = 0.2$.

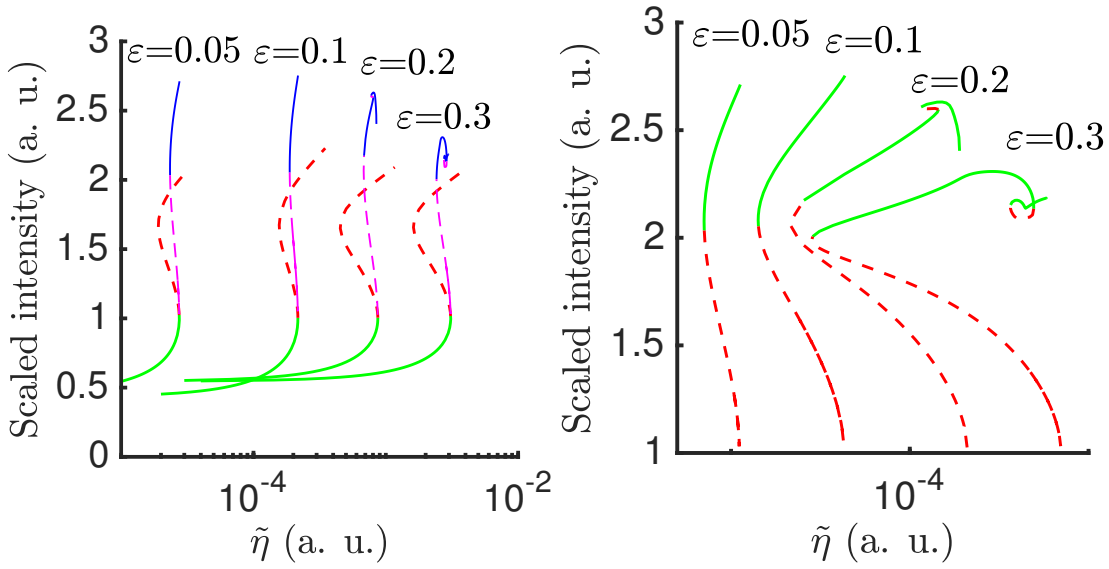


Figure 8: Bifurcation diagrams of Eq. (12) obtained for different values of $\varepsilon$. Left panel: CW states cut around S-shaped bifurcation curve (thick lines) and periodic solutions (thin lines). Solid lines represent stable states and dashed lines represent unstable states, $\tilde{\eta} = \eta - \eta_\varepsilon + \delta\eta(\varepsilon)$ is a shifted value of $\eta$. Right panel: Branches of periodic solutions from the left panel, magnified. The intensity is scaled by $\varepsilon^2$ and other parameters are as in Fig. 6.

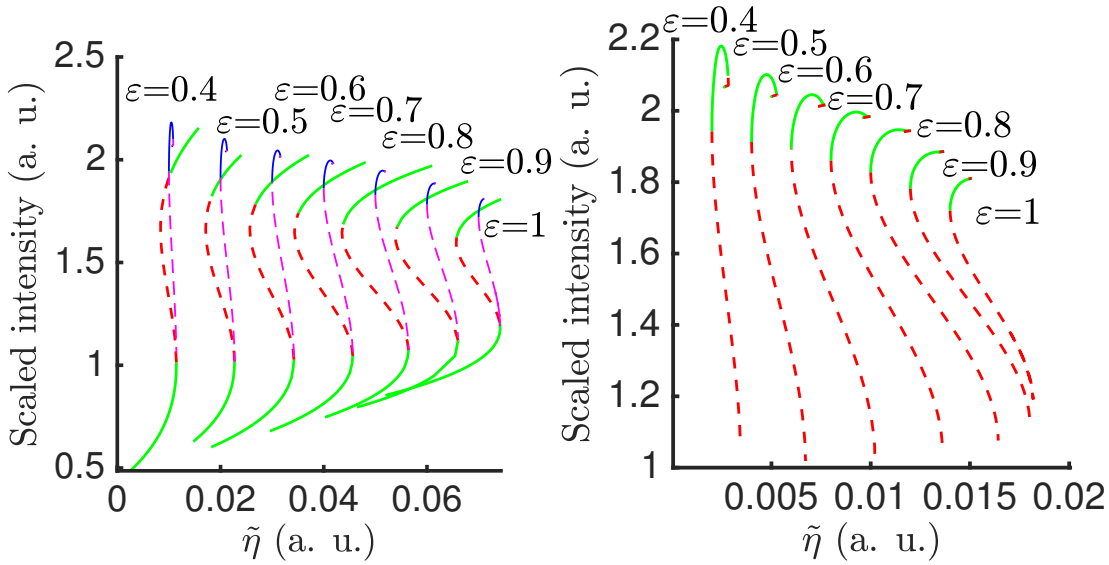


Figure 9: CW states cut around S-shaped bifurcation curve (thick lines) and periodic solutions (thin lines) of (12), where solid lines represent stable states and dashed lines represent unstable states. Right panel: Branches of periodic solutions from the left panel, magnified. The intensity is scaled by $\varepsilon^2$, the curves from left to right correspond to $j = 5, 6, 7, 8, 9, 10, 11$, and other parameters are as in Fig. 8.

Finally, let us study how the variation of the effective dispersion coefficient $\beta$ influences the existence range of the temporal localized structures. One can see in the top left panel of Fig. 11 that near the LLE

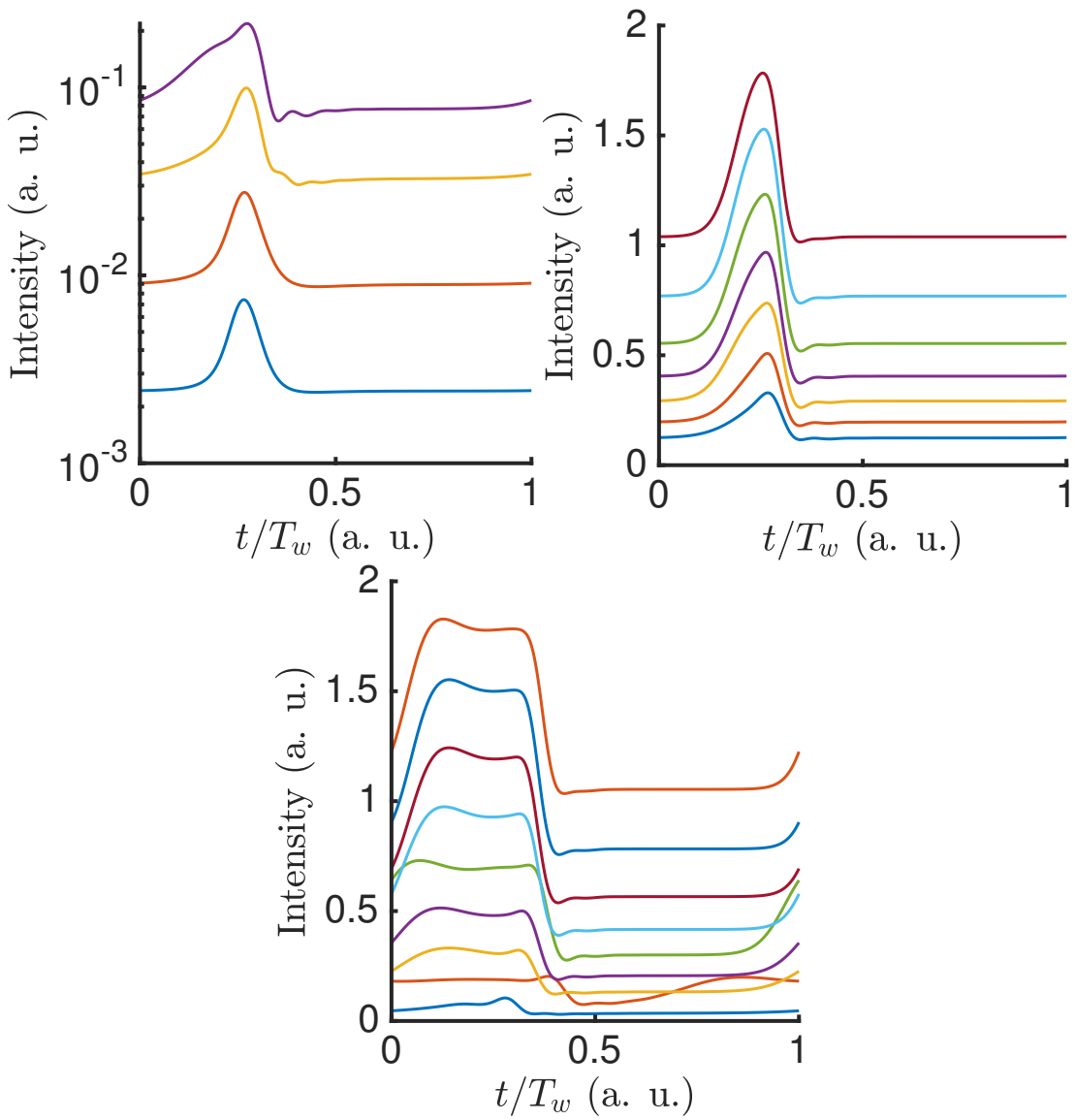


Figure 10: Top panels: Localized periodic solutions of Eq. (12) from the middle points of the stable parts of the branches depicted on Fig. 8, 9 for $\varepsilon$ increasing from 0.05 (bottom curve of the left upper panel) to 1 (top curve of the bottom panel). Bottom panel: Wider localized solutions from the secondary parts of the periodic solution branches for $\varepsilon$ increasing from 0.2 (bottom curve) to 1 (top curve). Time is scaled by the solution period $T_w \sim \varepsilon^{-1}$, which is controlled by the delay time $T$. Other parameters are as in Fig. 8.

limit ($\varepsilon = 0.05$) the localized solutions can be observed only for negative $\beta < -0.05$ corresponding to the anomalous dispersion regime. It is seen that when $\beta$ increases the interval of the injection rates between two fold bifurcations, where stable localized solutions exist, shrinks so that for $\beta \geq -0.06$ one can hardly see any stable localized structure in the region of S-shaped CW curve. However, by increasing $\varepsilon$ out of the LLE limit first to $\varepsilon = 0.3$ (top right panel of Fig. 11) and then to $\varepsilon = 0.5$ (bottom left panel), one can see that around $\varepsilon \approx 0.5$ localized structures can be observed for $\beta = 0$ as well. Furthermore, for $0.5 \leq \varepsilon \leq 1$ (bottom right panel) stable bright temporal dissipative solitons can be observed even with small positive $\beta$, $0 \leq \beta < 0.1$. Therefore, we conclude that out of the LLE limit temporal localized structures in the DDE model (12) could be observed not only in anomalous dispersion regime but also for positive $\beta$, although in a smaller range of the injection rates $\eta$. We

have considered here only one possible way to exit the LLE limit in a continuous manner, however our preliminary numerical simulations suggest that there are many possible combinations of values of $\kappa$, $\eta$, $\varphi$, and $\beta$ away from the LLE limit, where stable or unstable temporally localized structures can be observed. We leave this question to further studies, and, in particular, for experimentally justified parameters.

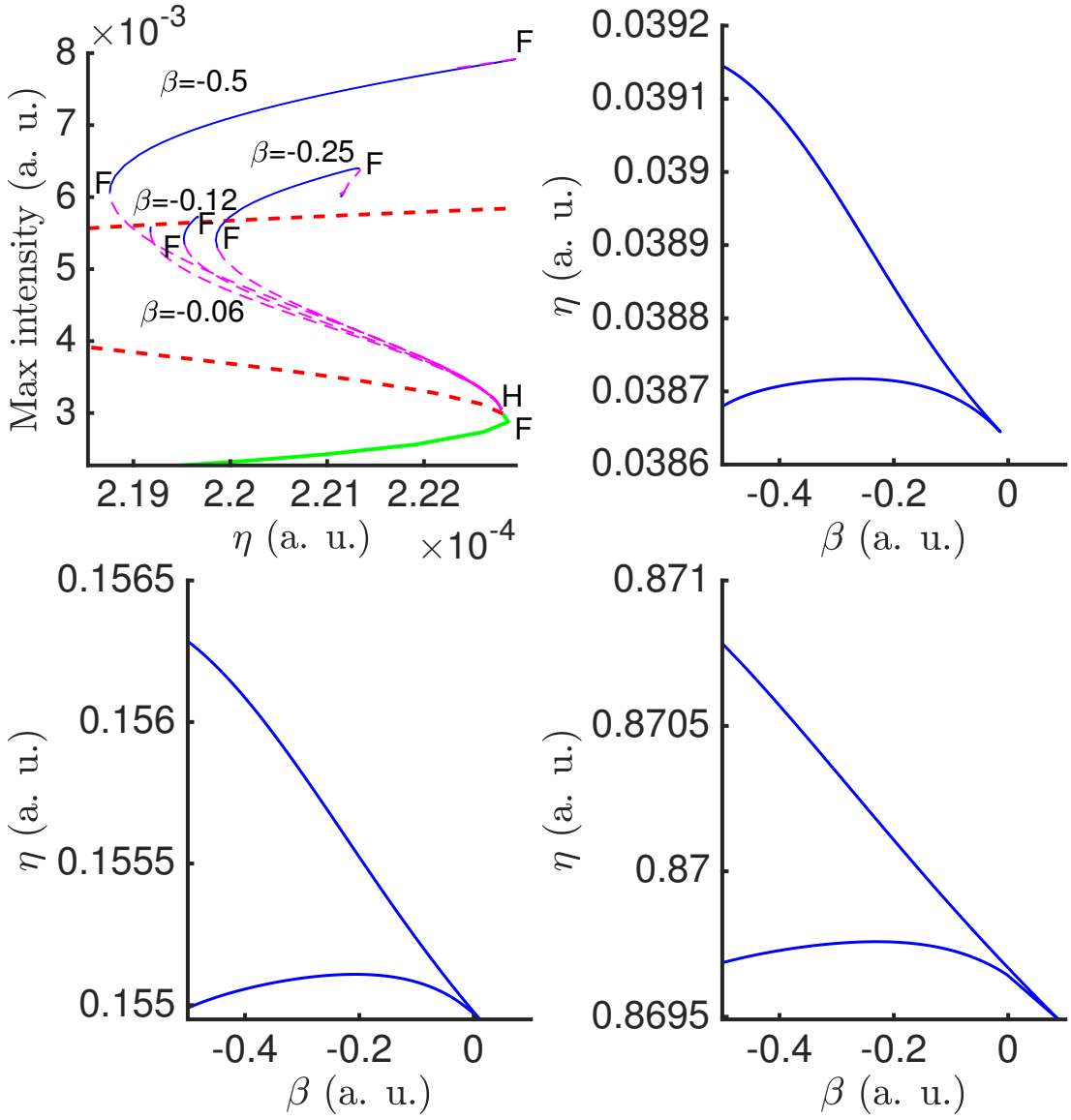


Figure 11: Top left: Bifurcation diagram of Eq. (12) for $\varepsilon = 0.05$ and various values of $\beta$. Thick lines indicate CW solutions cut around S-shaped bifurcation curve, while thin lines correspond to periodic solutions. Solid (dashed) lines represent stable (unstable) solutions. Fold bifurcations are marked by F and Hopf bifurcations are marked by H. Other panels show fold bifurcations of the localized periodic solutions of (12) on the plane of two parameters, $\beta$ and $\eta$. They correspond to $\varepsilon = 0.3$ (top right), $\varepsilon = 0.5$ (bottom left), and $\varepsilon = 1.0$ (bottom right). Other parameters are as in Fig. 8.

In this section we have demonstrated the existence of bright localized structures of the second oder DDE model (12). It follows from this result that such kind of structures should also exist in the original set of two DDEs (1) and (2). We can use this theory then to find parameters for (1)-(2) where localized structures exist (see Fig. 12).

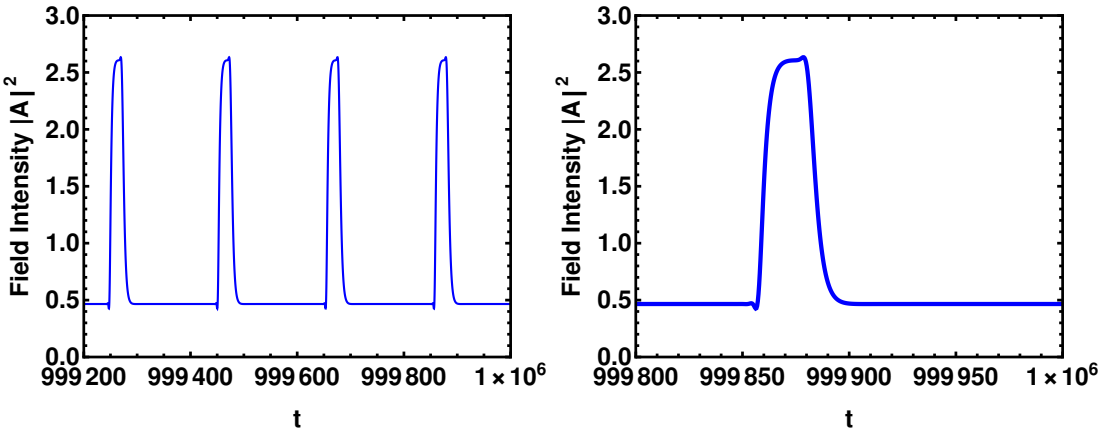


Figure 12: Periodic pulse train solution $A(t)$ of (1)-(2) (left) and single pulse (right), where the parameters are $\gamma_1 = 1, \omega_1 \approx 1.29, \gamma_2 \approx 0.26, \omega_2 \approx -0.034, \kappa_l \approx 0.68, \phi \approx -4.17, \eta_0 \approx 1.65, \alpha = 1.5, T = 200$. In the normalized equation (12) these values correspond to $\sigma = 3.23, \beta = 1, \kappa = 0.25, \varphi \approx -3.383, \eta = 1$.

## 5 Conclusion

We have considered a DDE model of an optically injected ring Kerr cavity with two spectral filters having different widths and central frequencies. We have derived a normalized complex-valued second order DDE (12), which is similar to real-valued DDE reported in [26]. This equation can be considered as a generalization of the Ikeda map, which explicitly contains second-order dispersion coefficient at zero frequency as a parameter. We have derived an admissibility relation for these parameters, analyzed stability of the CW solutions of this model in the limit of large delay, and demonstrated the effect of strong dispersion on the development of modulational instability. We have shown that in the limit of small losses and weak injection the DDE model can be reduced to a generalized version of the well known LLE, which is known to have dissipative soliton solutions. We have performed numerical bifurcation analysis of CW solutions and temporal localized structures using DDE-BIFTOOL package [30] and demonstrated qualitative similarity of the solutions of the DDE model with those of the LLE in the regime of anomalous dispersion ($\beta < 0$) in the corresponding limit. Moreover, out of LLE limit one can observe numerically stable localized structures not only in the anomalous dispersion regime, but also at zero and small positive values of $\beta$, albeit in a shrinkingly smaller interval of existence. Finally, these results demonstrate that chromatic dispersion caused by two suitably offset spectral filters in a nonlinear optical cavity can lead to instabilities and appearance of localized structures, which can be relevant for more complex systems with two filters such as Mamyshev oscillators.

# Appendices

## A MI in the LLE limit

Linear stability of the CW solutions of the classical Lugiato-Lefever equations was studied alalytically and numerically in a number of works, see e.g. Refs. [33, 34, 35] for both the normal and anomalous dispersion regimes. In this Appendix we consider the DDE model (12) in the LLE limit, where this

model can be reduced to the generalized LLE (16) with the additional diffusion (spectral filtering) term $(\sigma^2-2)/2$, which exerts a stabilizing effect on the CW solutions. A detailed linear stability analysis of the generaized LLE model (12) is beyond the scope of this paper. We present here only some analytical results concerning the sign change of one of the two quantities $\Lambda''_{\pm}(0)$ (see Eq. (25)), which can be a precusor of the MI.

Without the loss of generality we can assume that $\alpha = 1$ and $k = 1$. Substituting (14) and $A_0 = \epsilon u_0 + \mathcal{O}(\epsilon^2)$ into (23)-(25) and using $\Lambda_{\pm}(0) = -\operatorname{Re}\ln Y_{\pm}(0)$ we obtain:

$$\Lambda_{\pm}(0) = \varepsilon^2\left(1 \mp \operatorname{Re}\sqrt{\tilde{D}}\right) + \mathcal{O}(\epsilon^3), \quad \tilde{D} = -\left(\theta + 3u_0^2\right)\left(\theta + u_0^2\right), \tag{A.1}$$

$$\Lambda''_{\pm}(0) = 2 - \sigma \pm \operatorname{Re}\left[\frac{2\beta(2u_0^2+\theta)}{\sqrt{\tilde{D}}}\right] + \mathcal{O}(\epsilon). \tag{A.2}$$

where $\Lambda''_{\pm}(0)$ can be positive only when $\tilde{D} > 0$, i.e. for $-\frac{\theta}{3} < u_0^2 < -\theta$. We see from (A.1) and (A.2) that for $\tilde{D} > 0$ in the LLE limit we have $\Lambda_+(0) < \Lambda_-(0)$ and the curvature $\Lambda''_-(0)$ can be positive only for

$$\beta(2u_0^2 + \theta) < 0. \tag{A.3}$$

Let us consider the case when Eq. (20) has three real roots, which similarly to the standard LLE takes place for $\theta < -\sqrt{3}$. Taking a real root $u_0^2 = a^2$ of Eq. (20) we can express the remaining two roots as

$$u_{0\pm}^2 = \frac{1}{2}\left(\pm\sqrt{-4a^2\theta - 3a^4 - 4} - a^2 - 2\theta\right), \tag{A.4}$$

where three distinct roots are real for $\theta < -\sqrt{3}$ and

$$-\frac{2\theta}{3} - \frac{2}{3}\sqrt{\theta^2-3} < a^2 < -\frac{2\theta}{3} + \frac{2}{3}\sqrt{\theta^2-3}. \tag{A.5}$$

From this condition it follows that $2a^2 + \theta > 0$ for all $-\frac{4}{\sqrt{5}} < \theta < -\sqrt{3}$. Furthermore, the condition that $u_{0\pm}^2 < a^2$ for both the roots defined by (A.4) is also possible only for $2a^2 + \theta > 0$. Therefore it follows from (A.3) that for any $\theta < -\sqrt{3}$ the CW state with the highest intensity can have $\Lambda''_-(0) > 0$ only in the anomalous dispersion regime $\beta < 0$.

Since the condition $\Lambda''_-(0) > 0$ is not sufficient for the development of MI of a CW state, we assume further in (21) with $k = \alpha = 1$ that $\operatorname{Im}\lambda = \varepsilon w$. Then up to order $\varepsilon^2$ we obtain:

$$\Lambda_{\pm}(w) \approx -\left[2 + \frac{w^2(\sigma^2-2)}{2} \pm \sqrt{D(w)}\right]\varepsilon^2,$$

where $D(w) = -\left(u_0^2 + \beta w^2 - \theta\right)\left(3u_0^2 + \beta w^2 - \theta\right)$. We can find the frequencies $w$ at which the MI can observed using the conditions

$$\Lambda'_-(w) = 0, \quad \Lambda_-(w) = 0. \tag{A.6}$$

In particular, in the normal dispersion regime ($\beta > 0$) solving (A.6) with respect to $w^2$ and $\theta$ we obtain

$$w^2 \approx \frac{4}{\sigma^2-2}\left[\frac{u_0^2\beta}{\sqrt{4\beta^2 + (\sigma^2-2)^2}} - 1\right] > 0 \tag{A.7}$$

and two solitions for $\theta$

$$-\theta \approx \frac{u_0^2\left[2(\sigma^2-2)+\sqrt{4\beta^2+(\sigma^2-2)^2}\right]-4\beta}{\sigma^2-2} > 4, \tag{A.8}$$

$$-\theta \approx \frac{1}{\sigma^2-2}\left\{u_0^2\left[2(\sigma^2-2)+\frac{4\beta^2-(\sigma^2-2)^2}{\sqrt{4\beta^2+(\sigma^2-2)^2}}\right]-4\beta\right\} > 2\sqrt{3}. \tag{A.9}$$

Since according to (A.7), (A.8), and (A.9) both $w^2$ and $-\theta$ increase with $u_0$, the value of $-\theta$ corresponding to $w=0$ gives the lower bound of the detuning parameter, for which the development of MI is possible. We note that for $w=0$ and $\theta<0$ we have $D(0)<0$, and $\Lambda_-(0)\neq 0$, hence MI is not possible, and the lower bound obtained using $w=0$ is not tight and provides a necessary condition for the MI. It follows from Eq. (A.7) that for $w=0$ we get $u_0^2=\frac{\sqrt{4\beta^2+(\sigma^2-2)^2}}{\beta}>2$. Substituting this expression into (A.8) and (A.9) yields the following expression for the lower bound of the MI:

$$-\theta \approx \frac{2\sqrt{4\beta^2+(\sigma^2-2)^2}\pm(\sigma^2-2)}{\beta}, \tag{A.10}$$

where the sign "+"("−") corresponds to Eq. (A.8) [Eq. (A.9)]. The expression in the right hand side of Eq. (A.10) achieves its minimal value $-\theta\approx 2\sqrt{3}$ at $\sigma^2=2\mp\frac{2\beta}{\sqrt{3}}$. Therefore, for $-\theta<2\sqrt{3}$ MI is not possible in the normal dispersion regime.

From the previous paragraph we see that in normal dispersion regime the MI is possible only for sufficiently large $-\theta>2\sqrt{3}$. In the anomalous dispersion case ($\beta<0$) by solving Eq. (A.6) we get the following expression for the MI frequencies

$$w^2 \approx -\frac{4}{\sigma^2-2}\left[\frac{u_0^2\beta}{\sqrt{4\beta^2+(\sigma^2-2)^2}}+1\right] > 0$$

with $u_0>\frac{\sqrt{4\beta^2+(\sigma^2-2)^2}}{-\beta}>2$ and two solutions for the detuning parameter $\theta$:

$$-\theta \approx \frac{u_0^2\left[2(\sigma^2-2)-\sqrt{4\beta^2+(\sigma^2-2)^2}\right]-4\beta}{\sigma^2-2},$$

and

$$-\theta \approx \frac{1}{\sigma^2-2}\left\{u_0^2\left[2(\sigma^2-2)+\frac{-4\beta^2+(\sigma^2-2)^2}{\sqrt{4\beta^2+(\sigma^2-2)^2}}\right]-4\beta\right\}.$$

Here, the coefficients by $u_0^2$ can change sign depending on the parameters, hence there is no clear lower boundary for $-\theta$ in contrast to normal dispersion regime. Moreover, we could numerically observe MI for $\sigma=\sqrt{2.5}$, see Figs. 4, 5 Finally, we conclude that while it is possible to observe MI in the case of anomalous dispersion, in normal dispersion case that can be done only for sufficiently large $-\theta>2\sqrt{3}$.

# B Examples of MI out of LLE limit

Finally, we consider some examples of specific CWs, where relation (26) can be simplified, so that conditions for the change of curvature of $\Lambda_\pm(\xi)$ at $\xi = 0$ can be obtained explicitly, and then MI can be demonstrated numerically for close parameters.

For that, let us first study the conditions (27) and (28), which ensure that the CW is stable for $\beta = 0$ and that $\Lambda''(0)$ can become positive for some $\beta \neq 0$, and introduce auxiliary variable

$$\zeta = \cos\left(\alpha A_0^2 + \varphi\right),$$

in Eqs. (17) and (18). Then we get $\sin(\alpha A_0^2 + \varphi) = \pm\sqrt{1-\zeta^2}$ and Eq. (19) can be rewritten in the form $A_0 = \frac{\eta}{\sqrt{\kappa+1-2\sqrt{\kappa}\zeta}}$ with $-1 \le \zeta \le 1$.

For $\sin[2(\alpha A_0^2 + \varphi)] < 0$ using the relations (23) and (24) the inequalities (27) and (28) can be rewritten in the form

$$\frac{1-|\zeta|}{\sqrt{1-\zeta^2}} < \alpha A_0^2 \le \frac{1}{\sqrt{1-\zeta^2}}\left(|\zeta| + \frac{1+\kappa}{2\sqrt{\kappa}}\right). \tag{B.1}$$

Furthermore, from (26) one can see that for $\alpha A_0^2 > \frac{\sqrt{1-\zeta^2}}{|\zeta|} > \frac{1-|\zeta|}{\sqrt{1-\zeta^2}}$ we have $\mathcal{B} > 0$ when $\Lambda_+(0) < \Lambda_-(0) < 0$, and $\mathcal{B} < 0$ when $\Lambda_-(0) < \Lambda_+(0) < 0$. Hence it follows from (25) that the sign change of one of the two quantities $\Lambda''_\pm(0)$ corresponding to larger $\Lambda_\pm(0)$, which can lead to a MI of the CW solution, can occur only for $\beta < 0$. In the LLE limit one can see that this scenario usually corresponds to the change of the curvature sign of $\Lambda(\mu)$ of the upper part of the CW branch (see Fig. 3) in anomalous dispersion regime.

Alternatively, for $\frac{1-|\zeta|}{\sqrt{1-\zeta^2}} < \alpha A_0^2 < \frac{\sqrt{1-\zeta^2}}{|\zeta|}$ we have $\mathcal{B} < 0$ when $\Lambda_+(0) < \Lambda_-(0) < 0$, and $\mathcal{B} > 0$ when $\Lambda_-(0) < \Lambda_+(0) < 0$. Hence, in this case the sign change of the curvature can occur for $\beta > 0$.

For $\sin[2(\alpha A_0^2 + \varphi)] > 0$ instead of (B.1) we get the inequalities

$$|\zeta| + 1 < \alpha A_0^2\sqrt{1-\zeta^2} \le |\zeta| + \frac{1+\kappa}{2\sqrt{\kappa}}, \tag{B.2}$$

which imply that $A_0 > \frac{1}{\sqrt{\alpha}}$, which is incompatible with the LLE limit, where $A_0$ is asymptotically small. Since $|\zeta| \le 1$, from (24) one can see that for $A_0 = 0$ we have $D \le 0$. In particular, according to Eqs. (23) and (24) together with the inequality $\sin[2(\alpha A_0^2 + \varphi)] > 0$, for $D = 0$ we get $Y_\pm(0) = -\frac{1}{\sqrt{\kappa}}$ for $\sin(\alpha A_0^2 + \varphi) > 0$ and $Y_\pm(0) = \frac{1}{\sqrt{\kappa}}$ for $\sin(\alpha A_0^2 + \varphi) < 0$. Therefore, for larger $A_0$ and $D$ we have $\Lambda_-(0) < \Lambda_+(0) < 0$ for $\mathcal{B} > 0$ and $\Lambda_+(0) < \Lambda_-(0) < 0$ for $\mathcal{B} < 0$. Hence, it follows from (25) that in this case the change of curvature can be observed for $\beta > 0$.

Let us consider a simple case where $\varphi = -\alpha A_0^2 + \pi/2$ in Eq. (12) and, therefore, $\cos\left(\alpha A_0^2 + \varphi\right) = 0$ in Eq. (19). Hence, we get $A_0 = \frac{\eta}{\sqrt{1+\kappa}} < \eta$, which corresponds to the CW with the lowest intensity in case of bistable S-shaped CW branch. Furthermore, from (23) we obtain $D = \frac{\alpha^2\eta^4}{(\kappa+1)^2} - 1$ and $Y_+(0) = \frac{1}{\sqrt{\kappa}}\left(\frac{\alpha\eta^2}{\kappa+1} + \sqrt{D}\right)$. Therefore, from and (25) and (B.2) with sufficiently large $\beta$ we can have

$$\Lambda''_+(0) = 2 - \sigma^2 + \frac{2\beta}{\sqrt{\frac{\alpha^2\eta^4}{(\kappa+1)^2} - 1}} > 0, \quad 1+\kappa < \alpha\eta^2 < \frac{(1+\kappa)^2}{2\sqrt{\kappa}}.$$

This condition is reminiscent of the MI condition of a CW in the anomalous dispersion regime in the case of CW solutions of a semiconductor laser model [15], though second-order dispersion coefficient $\beta$ is multiplied here not by $\alpha$ but by a function of $\alpha, \eta, \kappa$. Similarly to the case of a laser under optical injection [16], this condition manifests the change of curvature of $\Lambda(\xi)$ at $\xi = 0$ for some $\beta > 0$, and it precedes appearance of a MI for larger $\beta$, which can be observed numerically (see Fig. 13, top).

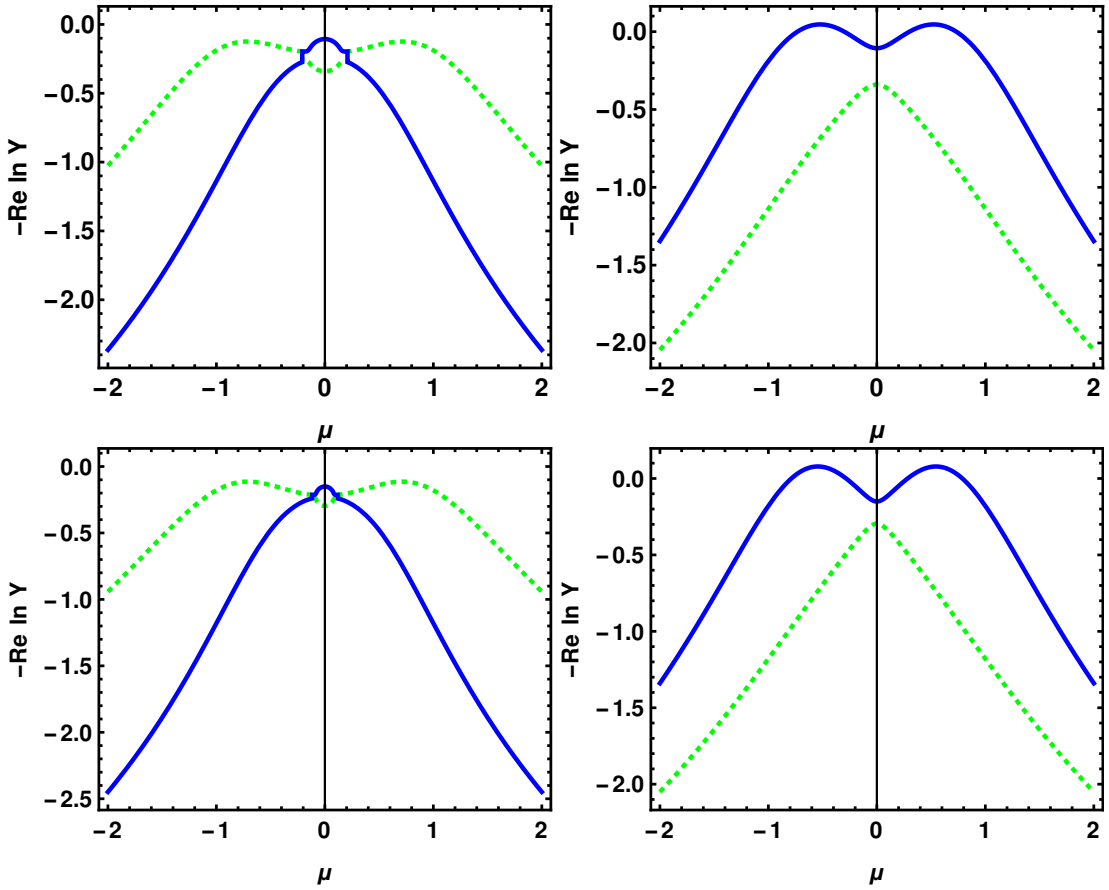


Figure 13: Curves of pseudocontinuous spectrum in the limit of large delay (21) of (12) of the CW with the lowest intensity $A_0 = \frac{\eta}{\sqrt{1+\kappa}}$ for $\zeta = \frac{\pi}{2}, \eta = 1.285$ (top) and the largest intensity (B.3) for $\zeta = \pi/6, \eta = 0.975$ with $\beta = -0.3$ (top-left), $\beta = 0.3$ (top-right), $\beta = -0.1$ (bottom-left) and $\beta = 0.1$ (bottom-right). Other parameters are $\kappa = 0.8, \sigma = \sqrt{2.5}, \alpha = 1$.

The most usual way to find a localized structure in form of a bright dissipative soliton, is to look for three coexisting CWs, where CW with the largest field intensity $A_0^2$ is modulationally unstable. Indeed, for $\varphi = -\alpha A_0^2 + \frac{\pi}{6}$, where $\zeta = \frac{\sqrt{3}}{2}$, the CW takes the form

$$A_0 = \frac{\eta}{2 - \sqrt{3}\kappa} \sqrt{3 + \frac{1 - \sqrt{3}\kappa}{\kappa^2 - \sqrt{3}\kappa + 1}} > \eta. \tag{B.3}$$

and the condition $\Lambda''(0) \geq 0$ takes the form

$$2 - \sigma^2 + \frac{2\beta\left(\sqrt{3}\alpha A_0^2 + 1\right)}{\sqrt{\alpha^2 A_0^4 - 2\sqrt{3}\alpha A_0^2 - 1}} \geq 0, \quad 2 + \sqrt{3} < \alpha A_0^2 \leq \frac{\kappa + \sqrt{3}\sqrt{\kappa} + 1}{\sqrt{\kappa}}.$$

Similarly, the change of curvature of $\Lambda(\xi)$ at $\xi = 0$ can occur only for $\beta > 0$, where also a MI can be observed (see Fig. 13, bottom). We can use the CW (B.3) by choosing corresponding parameter $\varphi$ to

find parameters where localized structures exist, and obtain parameters for the original system (1)-(2) to obtain these structures in numerical simulations (see Fig. 12)

## References


[1] Ikeda K 1979 Optics communications **30** 257–261

[2] Lang R and Kobayashi K 1980 IEEE journal of Quantum Electronics **16** 347–355

[3] Vladimirov A G and Turaev D 2004 Radiophys. & Quant. Electron. **47** 857–865

[4] Vladimirov A G and Turaev D 2005 Phys. Rev. A **72** 033808 (13 pages)

[5] Vladimirov A G, Turaev D and Kozyreff G 2004 Opt. Lett. **29** 1221–1223

[6] Viktorov E A, Mandel P, Vladimirov A G and Bandelow U 2006 Applied physics letters **88** 201102

[7] Viktorov E A, Mandel P and Huyet G 2007 Optics letters **32** 1268–1270

[8] Rossetti M, Bardella P and Montrosset I 2011 IEEE Journal of Quantum Electronics **47** 569–576

[9] Vladimirov A G, Kovalev A V, Viktorov E A, Rebrova N and Huyet G 2019 Physical Review E **100** 012216

[10] Vladimirov A G, Suchkov S, Huyet G and Turitsyn S K 2021 Physical Review A **104** 033525

[11] Vladimirov A G, Panajotov K and Tlidi M 2020 Optics Letters **45** 252–255

[12] Slepneva S, Kelleher B, O'shaughnessy B, Hegarty S, Vladimirov A and Huyet G 2013 Optics express **21** 19240–19251

[13] Slepneva S, O'shaughnessy B, Kelleher B, Hegarty S, Vladimirov A, Lyu H C, Karnowski K, Wojtkowski M and Huyet G 2014 Optics express **22** 18177–18185

[14] Heuck M, Blaaberg S and Mørk J 2010 Optics express **18** 18003–18014

[15] Pimenov A, Slepneva S, Huyet G and Vladimirov A G 2017 Phys. Rev. Lett. **118**(19) 193901

[16] Pimenov A, Amiranashvili S and Vladimirov A G 2020 Mathematical Modelling of Natural Phenomena **15** 47

[17] Schelte C, Camelin P, Marconi M, Garnache A, Huyet G, Beaudoin G, Sagnes I, Giudici M, Javaloyes J and Gurevich S 2019 Physical review letters **123** 043902

[18] Leo F, Coen S, Kockaert P, Gorza S P, Emplit P and Haelterman M 2010 Nature Photonics **4** 471

[19] Herr T, Brasch V, Jost J D, Wang C Y, Kondratiev N M, Gorodetsky M L and Kippenberg T J 2014 Nature Photonics **8** 145–152

[20] Lugiato L A and Lefever R 1987 Physical review letters **58** 2209

[21] Maleki L, Ilchenko V, Savchenkov A, Liang W, Seidel D and Matsko A 2010 High performance, miniature hyper-parametric microwave photonic oscillator 2010 IEEE International Frequency Control Symposium (IEEE) pp 558–563

[22] Matsko A B, Savchenkov A A, Liang W, Ilchenko V S, Seidel D and Maleki L 2011 Optics letters **36** 2845–2847

[23] Chembo Y K and Menyuk C R 2013 Phys. Rev. A **87** 053852

[24] Mamyshev P 1998 All-optical data regeneration based on self-phase modulation effect 24th European Conference on Optical Communication. ECOC'98 (IEEE Cat. No. 98TH8398) vol 1 (IEEE) pp 475–476

[25] Liu Z, Ziegler Z M, Wright L G and Wise F W 2017 Optica **4** 649–654

[26] Kashchenko I S 2008 Computational Mathematics and Mathematical Physics **48** 2172–2181

[27] Kolokolnikov T, Nizette M, Erneux T, Joly N and Bielawski S 2006 Physica D: Nonlinear Phenomena **219** 13–21

[28] Wolfrum M and Yanchuk S 2006 Physical review letters **96** 220201

[29] Yanchuk S and Wolfrum M 2010 SIAM J. Appl. Dyn. Syst. **9** 519–535

[30] Engelborghs K, Luzyanina T and Samaey G 2001 DDE-BIFTOOL v.2.00: A MATLAB package for bifurcation analysis of delay differential equations Tech. Rep. TW-330 Department of Computer Science, K.U.Leuven Leuven, Belgium

[31] Scroggie A, Firth W, McDonald G, Tlidi M, Lefever R and Lugiato L A 1994 Chaos, Solitons & Fractals **4** 1323–1354

[32] Leo F, Gelens L, Emplit P, Haelterman M and Coen S 2013 Optics express **21** 9180–9191

[33] Godey C, Balakireva I V, Coillet A and Chembo Y K 2014 Physical Review A **89** 063814

[34] Puzyrev D and Skryabin D 2021 Physical Review A **103** 013508

[35] Skryabin D, Fan Z, Villois A and Puzyrev D 2021 Physical Review A **103** L011502